A Double-Diffusive Interface Tank for Dynamic-Response Studies

Raymond W. Schmitt, Robert C. Millard, John M. Toole and W. David Wellwood

Department of Physical Oceanography
Woods Hole Oceanographic Institution

Abstract

A large tank capable of long-term maintenance of a sharp temperature-salinity interface has been developed and applied to the measurement of the dynamical response of oceanographic sensors. A two-layer salt-stratified system is heated from below and cooled from above to provide two convectively mixed layers with a sharp double-diffusive interface separating them. A temperature jump exceeding 10 ^{o}C can be maintained over 1-2 cm (a vertical temperature gradient of order 10^3 ^{o}C/m) for 1-2 weeks. A variable speed lowering system allows testing of the dynamic response of conductivity and temperature sensors in full size oceanographic instruments. An acoustic echo sounder provides non-disruptive monitoring of the interface and layer microstructure. Tests of several sensor systems show how the facility is used to determine sensor response times for the efficient design of lag-correction filters for the accurate computation of salinity. The effects of finite interface thickness, slow sensor sampling rates and the thermal mass of the conductivity cell are treated. Sensor response characterization is especially important for autonomous instruments where data processing and compression must be performed *in-situ*, but is also helpful in the development of new sensors and in assuring accurate salinity records from traditional wire-lowered and towed systems.

1. Introduction

The problem of matching the dynamic responses of temperature and conductivity probes for the accurate estimation of salinity dates back to the introduction of continuously recording profilers in the late 1960's. Usually, the temperature probe is the slower responding sensor, resulting in an under-estimate of the salinity when temperature is decreasing with time in the sensing volume, and an over-estimate when temperature is increasing. The resultant "salinity spiking" at high gradient interfaces has long been the focus of many data analysis efforts (e.g. Scarlet, 1975; Horne and Toole, 1980; Gregg *et al*, 1982; Gregg and Hess 1985; Giles and McDougall 1986; Ochoa 1989). However, it is not often appreciated that the lag correction problem is equally important for salinity computation whenever the sensors are moving in a temperature gradient. Even if salinity spikes are filtered from the data, the estimated salinity will be incorrect without a proper match between the response times of the temperature and conductivity probes. With traditional wire-lowered CTD instruments, it is common to tune the lag-correction algorithm after the fact, since the complete data times-series from all sensors is usually available. However, the increasing deployment of autonomous and/or expendable instruments requires characterization of sensor response prior to use, as satellite transmission of the raw time-series data is generally impractical. Moreover, *a priori* determination of response characteristics is useful for fine and microstructure studies as well as development of new sensors.

We are aware of only one other body of work that systematically studied the response characteristics of conductivity cells. This was performed in a salt-stratified tank, in which a sharp interface was maintained between two mixed layers by the turbulence generated by oscillating grids (Gregg *et al*, 1981, 1982, 1985). However, these tests failed to detect the substantial thermal mass

problems of one conductivity cell (Lueck and Picklo, 1990; Lueck, 1990), since there was little or no temperature difference across the salt interface in most of the experiments. Inspired by the sharpness of oceanic salt-finger interfaces that so clearly revealed the thermal mass problem to Lueck (1990), we have developed a simple technique for maintaining a very sharp temperature and salinity step between two mixed layers in a large tank using the principles of double-diffusive convection (Schmitt, 1994). In conjunction with a system for transiting CTD sensors through the interface at various speeds, the tank has proven to be very useful for determining sensor dynamic response characteristics. Since double-diffusive interfaces occur widely in the ocean, and provide some of the most challenging situations for salinity spiking, a CTD tuned for lag correction in this tank should perform well at sea. The system described is easy to maintain with modest energy input, so that a sharp interface with a large step in temperature and salinity is available for testing on a nearly continuous basis with minimal operator attention.

In section 2 the relevant principles of double diffusion are reviewed, followed by a description of the double-diffusive interface tank and its performance. Section 3 contains: a discussion of dynamic response tests with an example, the procedure for estimating the response time, its variation with fall-rate, the effects of finite interface thickness on the tests, the application of recursive filters to correct the data, and the effects of the thermal mass of the conductivity cell. Most sensor response results are presented for a CTD designed for a profiling float but the fall-rate response sensitivity is examined for standard CTD temperature sensors. A brief discussion of future work follows in Section 4. An appendix provides a relationship for adapting a single pole filter sensor response to the coarse temporal sampling often used in autonomous vehicles.

2. The Double-Diffusive Interface Tank

2.1 Double-Diffusive Theory

As Lueck and Picklo (1990) discovered, a thermohaline staircase is an ideal place to test the dynamic response of CTD systems. The characteristic mixed layers with near uniform properties separated by thin interfaces with strong gradients approximates ideal step changes in T and S with depth. Such staircases are maintained by double-diffusive convection (Schmitt, 1994). In the case studied by Lueck and Picklo, salt fingering was the active agent driving the convection. That is, both temperature and salinity decreased with depth, and the fact that the molecular diffusion of heat is 100 times faster than the diffusion of salt allows adjacent water parcels to come into thermal equilibrium while still having a substantial salinity difference. The resulting vertical convection releases energy in the unstable distribution of salt via centimeter-scale salt fingers in the high gradient interfaces (Stern, 1960). This unstable buoyancy flux in turn drives a large-scale overturning convection in the adjacent layers, keeping them well-mixed and uniform in properties (Stern and Turner, 1969). If the appropriate fluxes are maintained at the boundaries, then the layers remain well mixed and the interface remains sharp (Schmitt, 1979). However, maintenance of a boundary salt flux in the laboratory is problematic. The fluxes due to salt fingers are fairly large, and no one has yet achieved a steady state salt finger experiment even in small laboratory tanks. Also, a salt fingering interface is generally thicker than a "diffusive-convection" interface, and thus will not provide the thinnest interface possible. Finally, the microstructure of the fingers themselves would add a variable element to the interface T and S profiles.

To avoid many of the foregoing problems, the other form of double diffusion, the so-called “diffusive-convection” system, was chosen for our laboratory tank. This instability arises when

cold, fresh water lies above warm, salty (and denser) water. The salt distribution maintains the overall static stability while the faster diffusion of heat across the thin interface drives convection in the adjacent mixed layers. The theoretical potential for this instability was noted in a footnote by Stern (1960) and demonstrated in the laboratory by Turner and Stommel (1964). Salt is transported across a diffusive interface at a slow rate, allowing long duration runs in reasonably sized tanks. Also, it is straightforward to set up the two-layer salinity stratification and provide the boundary fluxes of heat, which is the driving agent for the diffusive convection.

Diffusive convection initially arises as an oscillatory "over stability" in contrast to the direct convective mode of salt fingers (Shirtcliffe, 1973). However, it quickly reaches amplitudes where steady convection is maintained in mixed layers by thermal conduction across a thin interface. The weaker salt diffusion acts as a brake on the system. When a stable salt gradient is heated from below (Turner, 1968), a series of mixed layers and interfaces forms staircase profiles in temperature and salinity. Heat supplied by intruded warm water at mid-depth is believed to cause the thermohaline steps observed in Arctic (Neal *et al*, 1969) and Antarctic (Muench *et al*, 1990) regions. The diffusive-convection system can be analyzed in terms of classic Rayleigh-Bernard convection, with the presence of salt delaying the onset of convection. The ratio of salt flux to heat flux is low (compared to salt fingers), since the transport across the interface is governed by molecular diffusion, so long as the stability is high.

The overall stability of a diffusive-convective system is governed by the density ratio, $R_\rho = \left(\frac{\beta \Delta S}{\alpha \Delta T} \right)$

where $\alpha = -\frac{1}{\rho} \frac{\partial \rho}{\partial T}$, $\beta = \frac{1}{\rho} \frac{\partial \rho}{\partial S}$ are the thermal expansion and haline contraction coefficients, and

ΔT, ΔS are the temperature and salinity differences across the interface. Fluxes are largest when R_ρ

is near one. Also, the ratio of salt buoyancy flux to thermal buoyancy flux approaches one in this limit, whereas at higher R_r it tends toward the square root of the salt to heat diffusivity ratio ($\sqrt{\frac{k_S}{k_T}} \cong 0.1$) (Veronis, 1968; Linden and Shirtcliffe, 1978). Thus, to preserve the temperature contrast in the tank as long as possible, it is most convenient to work at a high density ratio; which is achieved with a large salinity change (ΔS). Such a system is also easy to set up and maintain because of the large gravitational stability, and provides for sharp step-profiles lasting approximately two weeks of continuous running; longer if the thermal forcing is turned off during periods of non-use.

A double-diffusive system can be established by setting up a two-layer salinity stratification (salty water on the bottom) and subsequently heating the tank from below and cooling from above. The heating and cooling drives convection in the two layers, which keeps both well stirred and uniform in properties, without the need for oscillating grids. When fully developed, a sharp interface is maintained between the two layers, across which thermal conduction takes place, with little salt diffusion. This easily controlled heat flux maintains convection in both layers, and tank size can be as large as necessary to accommodate standard instrumentation. By traversing the CTD sensors through the tank at various speeds, one has an ideal test platform for investigating sensor response functions and tuning lag-correction algorithms. Since both temperature and salinity have a sharp jump across the interface, the influence of the thermal mass of the conductivity cell on measured conductivity can also be examined. The tank can also be used to quantify thermal transient effects on pressure gauges, other sensors, and the supporting electronics (the latter achieved by substituting fixed impedances for the sensors).

2.2 Tank Construction

Our present system shown in Figure 1, is a 4.7 m deep cylinder, 91.4 cm (3 ft) in diameter, with a 2.54 cm (1 in) wall thickness. This is a standard size poly-vinyl-chloride (PVC) waste-water pipe. The lower end is sealed with an anodized aluminum plate, 2.54 cm (1 in) thick. The working platform at the top of the tank is a 2.5 m x 2.5 m (8ft x 8ft) plywood deck constructed 3.6 m (12 ft) above ground level. A metal stairway and trapdoor provide access. The tank/platform assembly can be moved by forklift when the tank is empty.

The heating is supplied through a flexible mat resistive heating element (Electro-Flex Heat Inc., Bloomfield, Connecticut) held against the underside of the aluminum plate by foam insulation. It is powered by AC line voltage reduced through a variable transformer. Typically we dissipate about 400 W in the mat under the tank; the resistive mat is rated to 2200 W. Initial runs achieved temperature differences of 3-4 °C when only actively heating the lower layer. In such runs the upper layer would slowly warm and lose heat to the atmosphere causing the interface to weaken over time. Later, a cooling system was devised for the upper layer that allowed steady state temperature contrasts of 10-15 °C to be maintained for ~2 weeks at a time. The upper layer is cooled by a heat exchanger comprised of 2 lengths of coiled copper tubing mounted beneath closed cell foam, which acts both as floatation and insulation at the water surface. Cold water is circulated through the heat exchanger by a laboratory chiller (“Coolflow 75”, Neslab, Inc., Newington, N. H.), which has a rated capacity of 700 W. Heat losses out the sides and top of the tank are decreased by aluminized bubble wrap sheet insulation wrapped around the PVC pipe and the foam floatation at the surface. Application of 400 W of heating and cooling brings the lower layer to about 5 °C above room temperature and the upper layer to 5 °C below ambient temperature. Recently, the

substitution of a higher capacity chiller (Neslab “Coolflow HX-300”) has allowed the achievement of 15-20 ^{o}C temperature differences. If the tank is continuously heated/cooled with an initial salinity difference of order 10, then the temperature and salinity contrasts slowly decay and the stratification disappears in about two weeks. Cessation of heating and cooling slows the transfer of salt and preserves the stratification for several weeks. A sharp interface can then be obtained some 12-24 hours after restarting heating/cooling. The tank is located in a large "high bay" (for overhead clearance) that provides only crude regulation of the room temperature as the large garage doors are frequently open.

Fixed temperature and conductivity sensors (FSI digital OEM C-T sensors) are mounted through the tank sidewalls in removable fixtures to monitor temperature and salinity in the two layers. They are accessed via RS-232 interfaces connected to a laptop computer. Taps adjacent to the C-T sensors allow water samples to be drawn for salinity determination. The lower layer salinity is typically set to be 10-15 using commercially available “Sea Salt” manufactured by Lake Products Co. (Maryland Heights, Missouri), the upper layer is fresh water slowly introduced by trickling over a sheet of foam floatation. The upper layer salinity often starts out below the limit (~2.0) of the Practical Salinity Scale of 1978 (PSS78) but this condition does not affect the determination of thermometer time constants. A tap in the side of the tank located about 1.5 m below the top allows for selective withdrawal of fluid, normally of upper layer fluid. Also, when set-up with a simple siphon/overflow system, fresh water can be introduced to the upper layer so as to displace mixed water at the depth of the tap if the interface has thickened or if a decrease in upper layer salinity is desired.

The mechanism for dropping sensors through the interface uses an aluminum frame traversing the center of the tank as the holder for test CTDs. It is attached at each end to short sections of plastic piping (.635 cm i.d. PVC) gliding along taut nylon lines extending from an overhead frame to the bottom of the tank. Stainless steel springs (30.5 cm long) mounted around each line at the bottom serve to stop the framework before sensors can impact the bottom plate. Instruments are mounted to the frame and counterweighted by a variable number of oceanographic cable "messengers" attached to the other end of a thin steel cable (fishing line leader). This cable passes around a 0.5 m circumference pulley attached to a ten-turn potentiometer. A voltage divider circuit allows the potentiometer to be used as a depth scale. A metric tape measure extending the length of the counterweight travel tube (12.7 cm diameter clear plastic pipe (sediment core liner)) allows calibration of the depth scale. The fall-speed of the sensor frame is controlled by the payout of the data cable servicing the instruments on the frame. This is done using a 66 cm diameter bicycle wheel lined with double-sided tape. Its rotation rate is controlled by a variable speed 90V DC geared motor connected to the wheel by two seven-position bicycle sprockets and a drive chain. Available gearing allows the wheel to turn over nearly a tenfold range of ratios (0.3235 to 3.091) relative to the motor. Controlled speeds of 1 cm/s to 270 cm/s are possible with small, lightweight, sensors; the inertia and drag of larger instruments limits the speed attained. Most of our usage to date has been in the 10-100 cm/s range. The sensor and frame are counter-weighted to have a free-fall terminal velocity that is moderately greater than the desired test speed, so that the friction of the bicycle wheel on the data cable is sufficient to control the drop of the instrument. The other side of the data cable simply drapes down outside the tank. For our tests of float CTD heads, a conical plastic fairing was used to diminish the trailing wake of the flat end plate of the pressure housing.

This served to minimize the volume of fluid carried across the interface during runs, thus preserving the salinity contrast and helping to keep the interface thin.

Figure 1. The double-diffusive interface tank in the Clark Annex high bay. The PVC tank stands 4.7 m high and has an internal diameter of 91 cm. Aluminized bubble wrap provides insulation. A stairway at the rear provides access to the working platform. The speed of the bicycle wheel controls the fall rate of sensors through the sharp interface. The counter weights travel within the clear tubing to the right.

In order to assess the detailed structure of temperature and salinity profiles in the tank, a high-resolution microstructure probe is used. The probe ("Model 125 MicroScale Conductivity and Temperature Instrument" manufactured by Precision Measurement Engineering, Encinitas, Calif.) consists of a miniature 4-electrode conductivity cell in close proximity to a fast responding thermistor (FP-07). The cabling for the microstructure probes is bundled with the power and

communications cable for the test CTD (as needed; internally recording CTDs require no cable) and passed over the bicycle wheel. The microstructure and position data are digitized and logged at 200 Hz using a 16 bit A/D converter on a PCMCIA card in a laptop computer. A Butterworth filter with cutoff at 100 Hz prevents aliasing of the digitized micro-structure data. The CTD data is monitored using a digital RS 232 communications line to the laptop; a number of different sampling rates have characterized the CTD units tested to date, and they are sometimes run in an internally recording mode, with data offloaded after each run, in order to achieve the fastest sampling rate.

Because the passage of a test CTD causes some disruption of the interface and produces microstructure in the mixed layers, successive runs must be spaced in time. To establish when it is appropriate to make the next run, it is desirable to monitor the state of the interface non-invasively. We found that an inexpensive commercial echo sounder was helpful in this regard. The unit used is a “Fishfinder 240” (Garmin, Inc. Olathe, Kans.); it has a 200 kHz frequency and a narrow beam transducer (12 degree), to minimize echoes from the sides of the tank. The backscattered acoustic returns are caused by the sound-speed variations produced by temperature and salinity gradients in the tank. The position and intensity of the interface, convective plumes moving in the layers due to heating and cooling, and the microstructure generated by passage of the test sensors are all easily discernable. This allows one to gauge the readiness of the tank for additional tests without disturbing the interface with a probe. Further experimentation with more quantitative acoustical tools is underway to help characterize the strength of backscatter return from microstructure as a function of frequency.

2.3 Tank Performance

The intensity of the interfacial temperature jump is set by the heat flux within the tank. Sample temperature and conductivity profiles from the microstructure probes are shown in Figure 2 for a setup with heating below and cooling above. CTD sensors were profiled through the interface at an average speed of 7.5 cm/s; figures 2.c and 2.d illustrate the fall rate and depth variations for this drop. The overall layer homogeneity and the sharpness of the interface is revealed by the microstructure probes (Figure 2.a, 2.b), which are calibrated for each run against the fixed C-T sensors in each layer. The temperature change of nearly 10 ºC was achieved over ~1.5 cm: a vertical temperature gradient of 700º C/m (Figure 2.b). The change in conductivity was nearly 20 mS/cm, and the more rapid response of the microstructure conductivity probe relative to the temperature sensor can be seen.

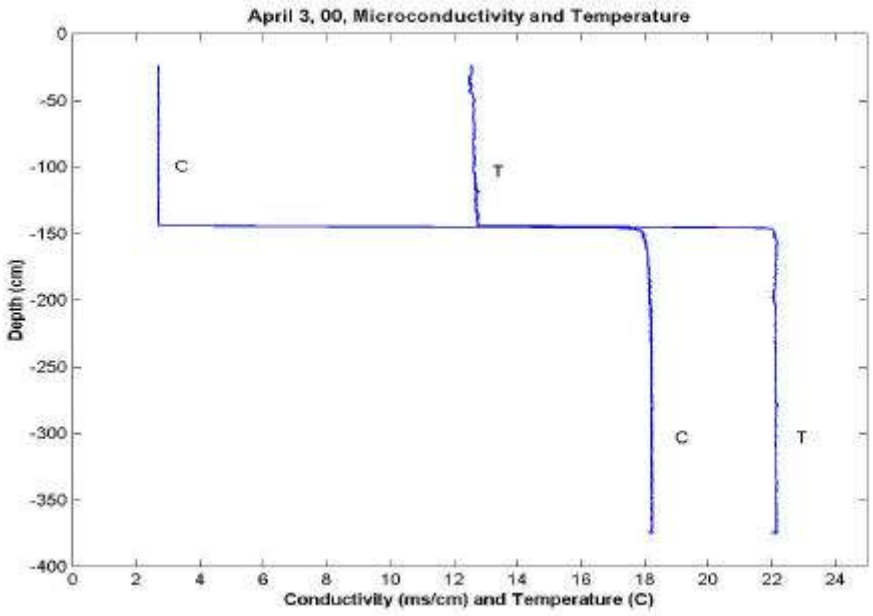

Figure 2a Profiles obtained with the microstructure sensors of conductivity and temperature through the double-diffusive plunge tank from April 3, 2000.

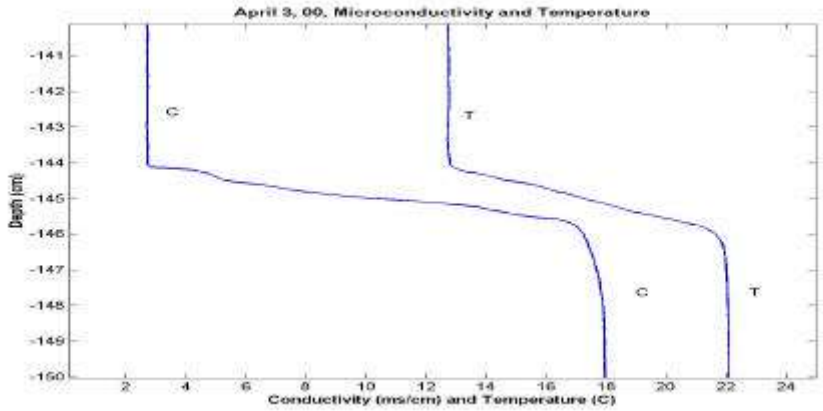

Figure 2b. Expanded view of the interface between the two layers for the April 3 run. The interface is little more than 1 cm thick; the temperature gradient is approximately 700°C/m.

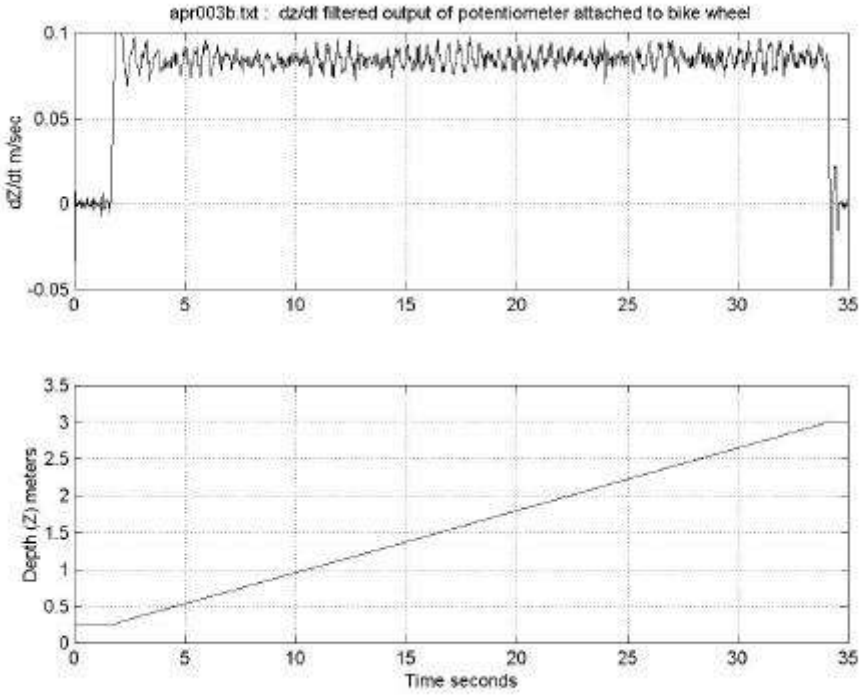

Figure 2 c & d Displacement (lower) and filtered drop rate (upper, oscillations are filter artifact) versus time for a run on April 3, 2000.

The large temperature gradient obtained across the double-diffusive interface is consistent with molecular conduction being the primary means of heat transport from the lower to the upper layer. That is, we can estimate the conductive heat flux from the observed gradient, the thermal conductivity of sea water (k_T = 1.424 x 10^{-7} m^2/s) and the tank area (A=0.66m^2):

$$Q = A\rho C_p k_T \frac{dT}{dz} \quad . \qquad 3.1$$

For the estimated interfacial temperature gradient of 700 °C/m, the calculated heat flux is 272 Watts. This indicates that nearly 70% of the 400 Watts of heat supplied to the lower layer was transmitted through the interface in this run, with the remainder presumably lost through the tank sidewalls and the external area of the aluminum bottom plate, since the layer temperatures were approximately constant.

The sharpness of the interface, and the homogeneity of the mixed layers, means that probes dropped through the tank will experience a step change in temperature (and salinity), particularly since the sampling volume of most sensing systems is larger than one centimeter. In some of the following analysis we utilize the observed sharpness of the temperature interface to assume a step temperature response solution rather than using the observed microstructure temperature sensor forcing to find the response. The effect of a finite width step is examined later.

3. Dynamic response tests

3.1 General considerations

The task of computing salinity from measurements of temperature and conductivity is complicated by their differing responses due to: (1) simple time delays or lags due to physical positioning of the probes or electronic digitization sequence, (2) the time it takes the sensors to respond to changes in the environment, and (3) impacts the probes themselves have on the measurement (such as effects due to the thermal mass of conductivity cells). Also, we must expect that all of these issues will be speed dependent. Both conductivity cells and temperature sensors introduce filtering but there is an intrinsic difference in the nature of their responses; the temperature sensor introduces a phase shift while the conductivity sensor does not. The primary conductivity response is simply due to

the flushing of the sample volume by movement of the cell through the water. This produces a sensor response that is, to first-order, a boxcar filter having a filter length in time (τ) equal to the effective flushing length of the cell (L) divided by the instruments fall rate (w); $\tau = L/w$. The boxcar filter introduces no phase shift as a function of frequency (ω) to the conductivity data but does reduce the amplitude of the conductivity variations as $\mathrm{sinc}(\omega\tau)$. The effective flushing length is approximately the cell length, although Topham and Perkins (1988) discuss conditions under which the flushing length can be greater, such as when the field of a cell extends beyond the cell itself, as is the case with the inductive cell examined here. By contrast, the temperature sensor involves the diffusion of heat through a fluid boundary layer and the physical structure of the probe. This introduces a delayed response in the measured temperature signal. One scheme for matching the response characteristics of the two probes is to apply a recursive filter to the conductivity data to impose a phase shift similar to that of the temperature probe. On the other hand, when filtering temperature to match the flushing time of conductivity, we recommend filtering the temperature channel with a boxcar filter having no phase shift, rather than a recursive filter as suggested by Giles and McDougall (1986). Also, their suggestion for matching of the sensor's time constants at a certain drop speed is not effective without corrective filtering to account for the phase shift with frequency in temperature not found in conductivity.

3.2 An example

A number of instruments including CTD systems manufactured by Seabird Electronics, (Bellview, Wa.), Falmouth Scientific Incorporated (FSI, Cataumet, Ma.) and Idronaut (Brugherio, Italy) have been evaluated in the dynamic response tank. Here we limit the discussion of results primarily to the EXCELL CTD current being developed by FSI for use on profiling floats and include examples with and without the additional thermal contrast provided by the chiller.

Profiles of temperature, conductivity, salinity and density were obtained from a number of float CTDs; an example from EXCELL s/n1318 traversing through the tank interface at a speed of 16.5 cm/s is shown in Figure 3a-d. No chiller was used in the upper layer and therefore only a modest temperature change of about 4°C was achieved. For this run, the normal lag-correction filtering within the EXCELL has been disabled to illustrate the raw sensor response. The temperature (upper panel) probe clearly has a much slower response than the conductivity (solid curve in 2nd panel). Temperature exponentially approaching the lower layer temperature value over ~1.0 m causes incorrect salinities and densities to be calculated in the transition region. The density profile (bottom panel) overshoots in the transition to produce an apparent density inversion.

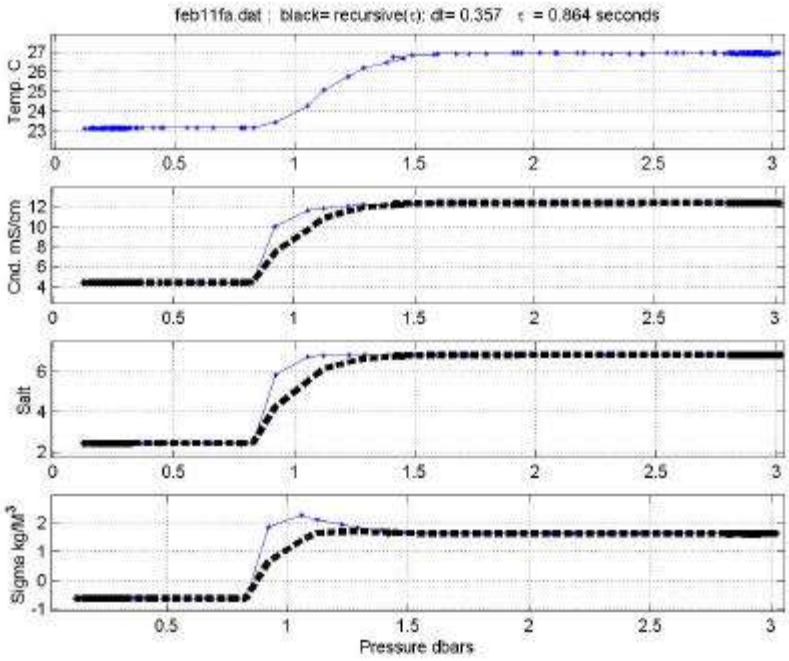

Figure 3 a-d Four panel plot of temperature, conductivity, salinity, and density versus pressure from the first 11 Feb. plunge EXCELL # 1318. Panels b, c, and d have over plots of no lag (= solid); recursive filtered (= dashed). Note the density overshoot for solid (no lag) curve around 1 decibar associated with the step in temperature and salinity corrected by the filter. The EXCELL's raw pressure data is used as the horizontal axis, rather than measured depth, which accounts for the irregular spacing of the points.

The 1978 Practical Salinity Scale (PSS78) (Unesco, 1981) is used to calculate salinity from measurements of conductivity, temperature, and pressure. Accurate salinity calculation requires conductivity, temperature and pressure data with matched response characteristics. The temperature response is controlled by the ability of the temperature probe's housing and surrounding boundary layer to lose or gain heat. One of the simplest models for describing the response of a temperature probe is the single pole filter equation (Fofonoff *et al*., 1974):

$$\frac{dT(t)}{dt} = \frac{1}{\tau}\left(T_o(t) - T(t)\right) , \qquad (3.2)$$

where $T(t)$ is the time series of measured temperature, $T_o(t)$ is the time series of ocean temperature, and τ equals the temperature probe response time.

Fofonoff *et al*. (1974) described a technique for speeding up the temperature measurement by rearranging equation (3.2) to solve for the ocean (true) temperature. They recommended estimating the temperature gradient $\frac{dT(t)}{dt}$ by linear least squares. Fofonoff *et al*. (1974) found that three observations in time were the optimum number of temperature values for estimating the gradient, but that further smoothing was usually required. A drawback to speeding up temperature is an increased temperature sensor noise level proportional to the magnitude of the response time (τ). In the formulation below, we solve equation (3.2) for the response of temperature probe in order to compare its response characteristics (phase in particular) to a recursive filter lag correction technique that delays the conductivity sensor data to match the response of temperature. Middleton and Foster (1980) first suggested this approach, which is generally preferred over speeding up the temperature for most applications where resolution of finestructure is not required. An appendix shows the derivation of the recursive filter lag weights for the case of slow sampling rates often

used with CTDs on autonomous instruments where the instrument sampling period approaches or in some cases exceeds the temperature sensor response time.

3.3 Estimation of sensor response time

The simplest model for the temporal response of a temperature sensor is a low pass filter described by the solution to equation 3.2. The step response for a temperature change from T_0, the initial temperature, and the final temperature (T_f) is given by:

$$T(t) = T_0 + (T_f - T_0) \cdot (1 - e^{-\frac{t}{\mathrm{t}}}) \tag{3.3}$$

We define the time origin (t=0) to be at the top of the interface. By rearranging and taking the natural logarithm, we get:

$$\log\left[\frac{(T_f - T(t))}{(T_f - T_0)}\right] = -\frac{t}{\mathrm{t}} \tag{3.4}$$

The temperature time series $T(t)$ from a plunge test can be fit to equation 3.4 using a linear Least Squares Regression (LSR) procedure. The slope of the least squares fit of $\log\left[\frac{(T_f - T(t))}{(T_f - T_0)}\right]$ against time yields the temperature sensor time constant $(1/\mathrm{t})$ while the intercept or bias is interpretable as an offset from the assumed time origin. Note that the data being fit involves $\log(T_f - T(t))$ which becomes indeterminate when the temperature $T(t)$ reaches T_f, so care must be exercised to exclude these data from the LSR.

As an example we consider the Falmouth Scientific EXCELL CTD, which is designed for profiling floats. The EXCELL temperature probe consists of a 100-ohm platinum wire element pressure protected by a thin-walled cylindrical titanium housing mounted adjacent to the conductivity cell at its centerline and separated horizontally by approximately 3.0 cm from the conductivity cell axis.

The temperature probe thus does not sense the temperature of the volume of seawater inside the cell; in our analysis we neglect any real differences in the water temperatures inside and immediately adjacent to the cell due to microstructure.

The EXCELL CTD is an autonomous instrument with a relatively coarse sampling interval of Δ = 0.35 s. This compares with a typical ship-lowered CTD system such as the Mark IIIC CTD with Δ = 0.03 s or the SBE 911 plus with Δ = 0.04 s The EXCELL employs an inductive conductivity cell made of alumina with a length and external diameter of 4.5 cm and internal diameter of 2.4 cm. The conductivity sensor measures the seawater conductance in the cell interior with a smaller contribution from the surrounding seawater. Ship-lowered CTD systems have a typical lowering rate of 100 cm/sec, which would give a minimum flushing time of 0.045 seconds for the EXCELL conductivity cell. The EXCELL CTD as used on the PALACE float vehicle has a typical ascent speed of ~10-20 cm/s (Davis *et al*., 1992) which translates into a flushing time of ~0.45 seconds; thus, each conductivity sample from a float is roughly independent.

The results of four runs with EXCELL CTD s/n 1318 on February 11, 2000 are summarize in Table I The drop rate for the four runs was 16.5 cm/s and varied by less than 5 percent. The first run is plotted in figure 3 a-d. The dashed curves apply the LSR response time (t =0.864 s) of Table I to conductivity using the recursive filter given in formula (5.1). This eliminates the apparent density instabilities of the density profile (dashed curve of figure 3 d) noted earlier.

The fitting procedure to the EXCELL temperature sensor data gives response times that are repeatable to within 5% and suggest that the single pole filter model produces a fairly reliable

estimate of the lag adequate for correcting slow sampling rate (2 to 3 Hertz) CTD systems, provided the fall rate is not too variable. However, data collected with this technique is also suitable for developing more sophisticated transfer functions, for example (Horn and Toole, 1981), should they be required in more rapidly sampled data systems.

Table I

Four successive lowering of EXCELL s/n 1318 on Feb. 11, 2000. Response time (τ) and the bias columns are from the LSR using equation 4.3 over 5.75 seconds of data beginning at the maximum sensed temperature gradient. The last 3 columns are data from the microstructure C / T sensors that demonstrate the sharpness of the interface vertically. Passage of the CTD degrades the intensity of the temperature gradient in successive runs but these still provide useful estimates of the thermometer response time.

Run #	Response time (τ) s	bias s	Δz meters	ΔT C	dT/dz C/m
1	0.864	0.0411	0.024616	3.6886	149.8461
2	0.885	0.0092	0.059631	3.1939	70.3319
3	0.912	-0.0382	0.07868	3.0439	38.6868
4	0.950	0.0136	0.073904	2.8105	38.029

To estimate the model coefficient (t) the least squares regression procedure uses temperature data beginning at the time of maximum sensed temperature gradient and includes temperature values for several time constants beyond. Our estimating procedure for the response time was found to be sensitive to the data interval used, with the estimate increasing as the data interval increased. The fit coefficient becomes unreliable as the sensor temperature $T(t)$ approaches T_f as discussed earlier. We find that the best estimate corresponds to the t value having the LSR time bias value nearest to zero (see example that follows). We settled on 16 observations, approximately 5.75 seconds of data or 6-7 lag intervals, for the estimates shown in Table I. A bias of zero, within the uncertainties of the sampling interval of 0.357 s, indicates the response time (t) is optimal.

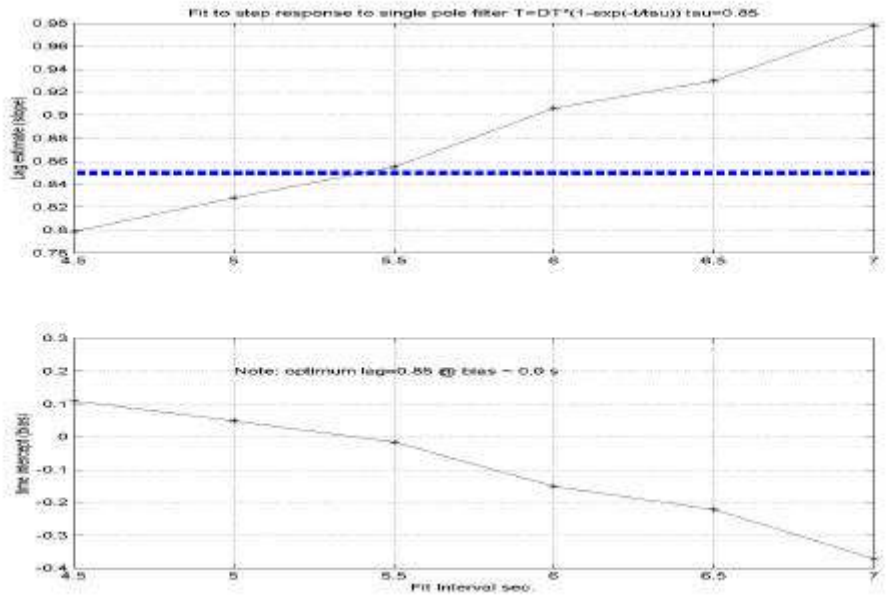

Figure 4 a-b Illustration of bias =0.0 time offset producing optimum response time estimate for exponential data simulation using τ=.85 s, fit for slope = $1/\tau$ (upper) and bias= time offset (lower panel) plotted versus fitting interval in seconds (for 2.8 hz sampling interval).

To further illustrate the idea of minimizing the time bias estimate to obtain the optimum lag estimate, we examined the accuracy of the fitting process when applied to a time series derived from a known exponential form. An artificial temperature time series was generated using equation 3.3 subsampled at 2.8 hertz with a known time constant τ = 0.85 s. LSR fits to eqn. 3.4 were then done over various time intervals from the known start of the temperature step; the estimated slope ($1/\tau$) and bias are plotted in figure 4 a-b. Figure 4 a-b illustrates that the best estimate to the response time (τ) corresponds to the bias estimate closest to zero that, in this case, happens to be for a fit interval of 5.5 seconds.

3.4 Response time variations with fall rate

We have explored the effect of drop rate on the temperature sensor response using a pair of Idronaut CTD temperature sensors. Two temperature sensors mounted vertically to the flow were

successively lowered four times with drop rates ranging from 0.13 m/s to 0.68 m/s. The sample rate for the Idronaut is 12 Hertz which provides roughly a factor of five faster time resolution than is achieved with the EXCELL CTD. Plots of the output for both temperature sensors are shown in figures 5 a-b together with the LSR single pole model output and the temperature step. Both temperature probes appear well described by the single pole model at a drop rate of 0.47 m/s and the derived response time values of the probes are matched to within 0.01 seconds. The results of these four drops, figure 5 c-d, shows a large variation in the estimated time constant as a function of drop rate (w) for both temperature sensors. The observed fall rate scaling of $w^{-1/2}$ is expected from the behavior of high Reynolds number boundary layer thickness (Gregg and Meagher, 1980). It was observed in the plot of the temperature versus time for the slowest (0.13 m/s) lowering rate, that both temperature probes deviated from the idealized exponential single pole filter behavior, likely due to the lower Reynolds numbers.

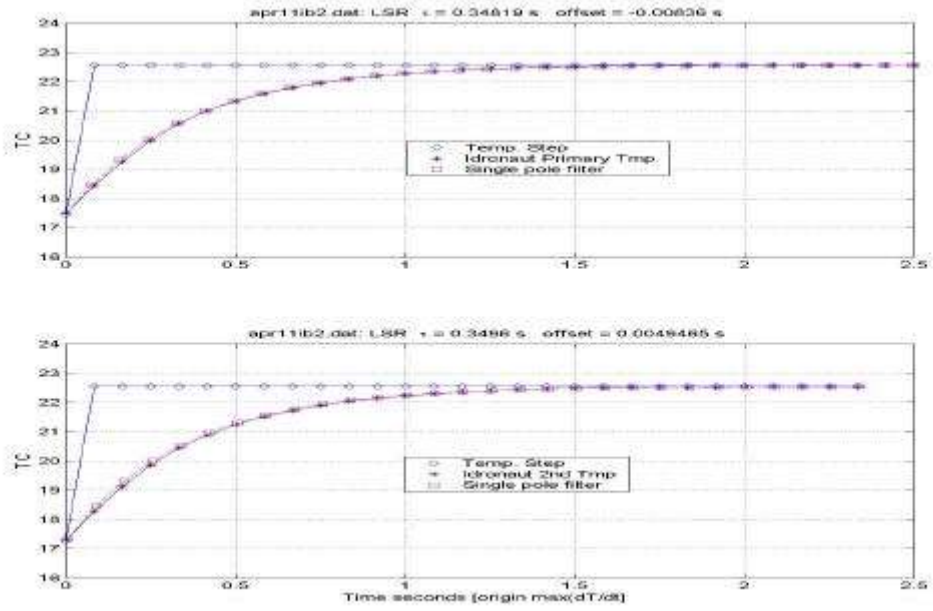

Figure 5 a-b: Plot of response of Idronaut primary temperature probe (*) (upper panel) and Idronaut 2nd temperature probe (*) (lower) both panels show step temperature change (◊) and model response ( ) for time constant (t) shown.

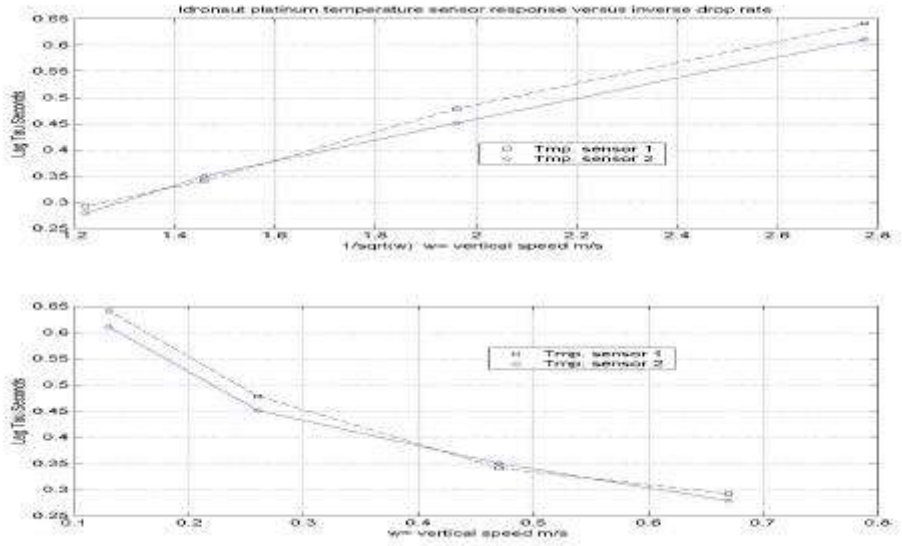

Figure 5 c-d Plot of time constant τ versus lowering rate (w) (bottom panel) and τ versus $w^{-1/2}$ (upper panel), a high Reynolds Number scaling with lowering rate (Gregg and Meagher, 1980).

3.5 Finite step effects

We also consider the effect of a non-ideal step on the sensor response. Repeated runs in the tank can thicken the interface to 10 cm or more (Table I) if there is insufficient time between runs to allow the convection to redevelop a sharp interface. The time record of a temperature transition through a thick interface (of thickness *H* and drop rate *w*) can be represented by a linear ramp between T_0 and the final temperature T_f over an interfacial transit time (= *H/w*):

$$T = T_0, for t < 0 \tag{3.5}$$

$$T = \left[\frac{T_f - T_0}{\frac{H}{w}} \right] \cdot t, for 0 < t < H / w$$

$$T = T_f, for t > H / w.$$

The single-pole temperature sensor response (T_r) for time constant (τ) to the above temperature time variation is:

$$
\begin{aligned}
&for\, t < 0: \\
&T_r = T_0 \\
&for\, 0 < t < H/w: \\
&T_r = K \cdot e^{-\frac{t}{\tau}} \cdot \left[\tau + (t - \tau) \cdot e^{\frac{t}{\tau}} \right] \\
&for\, t > H/w: \\
&T_r = K \cdot \frac{H}{w} + \left[T_i - K \cdot \frac{H}{w} \right] \cdot \exp\left[\frac{t - \frac{H}{w}}{\tau} \right] \\
&where \\
&K = \left[\frac{(T_f - T_0) \cdot w}{H} \right], and \\
&T_i = K \cdot e^{-\frac{H}{\tau w}} \cdot [\tau + (\frac{H}{w} - \tau) \cdot e^{\frac{H}{\tau w}}].
\end{aligned}
\tag{3.6}
$$

The temperature response for a discretely sampled data series, traversing interfaces of increasing thickness (H), are plotted in figure 6a. Fig 6.b displays the rate of change of sensed temperature; the maximum temperature gradient is increasingly displaced from the start of the interface as the interface thickens. The position of the maximum gradient is close to *H/2*. It was found that LSR fits to these analytic ramp temperature profiles tended to yield estimates of the time constant that were overestimated from the assumed step temperature change, consistent with the trend observed in Table I. Thus, best practice is to use runs where the interface is sharp, or take the overestimate of the time constant expected from a thick interface into account when designing the corrective filter.

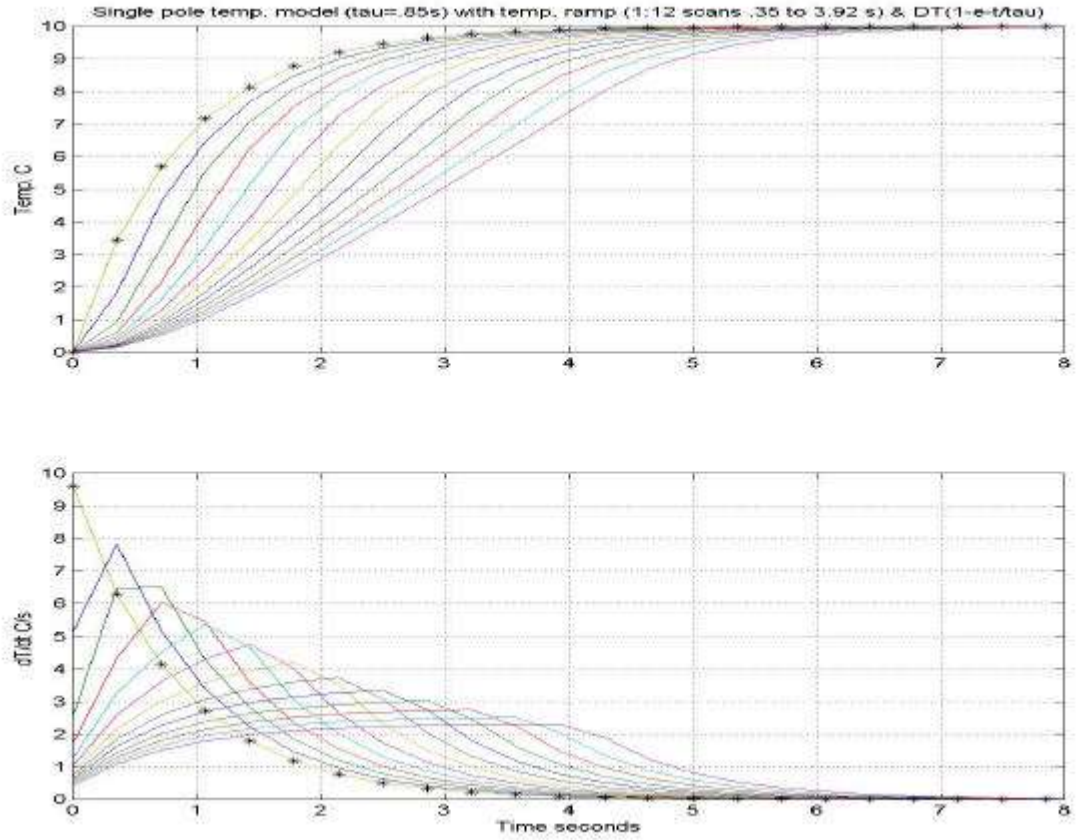

Figure 6 a-b Upper panel is sensed temperature versus time for longer ramping intervals and lower panel shows maximum temperature gradient delayed increasing time intervals until temperature ramp end

3.6 Application of sensor response correction

Having determined the response time of a temperature probe, one must devise a scheme to match the responses of the conductivity and pressure sensor data. One common approach is to digitally filter the conductivity and pressure data to yield a response comparable to that of the temperature channel. This is readily done using a recursive filter to introduce the needed phase shift, such that:

$$C(t) = \mathrm{a} \cdot C(t - \Delta) + (1 - \mathrm{a}) \cdot C_0(t) \qquad (3.7)$$

where

$C(t)$ the time series of filtered conductivity,

$C_o(t)$ the time series of observed conductivity,

Δ is the sample interval, and

a is a weight related to the temperature sensor time constant.

The formula for a found in Bendat and Piersol (1971) and also used in Millard (1982) is

$$a = e^{-\Delta/t} \tag{3.8}$$

This formulation is valid when the sample interval is short compared with the sensor response time (*i.e.*, $t << \Delta$). A better estimate for the weight a for the case of the sampling interval approaching the response time (*i.e.* for slowly sampled instruments such as the EXCELL CTD) is

$$a = \frac{1}{(1+\Delta/t)}. \tag{3.9}$$

The derivation of this expression for a is given in the appendix. This expression is nearly equivalent to eq. 3.8 for $\Delta << t$ and is superior when $\Delta \sim t$, so we recommend it as the more general relation.

An example with EXCELL CTD data collected on April 3, 2000 having the conductivity data filtered with the instrument default lag value corresponding to t = 0.94 seconds is shown in figures 7 a-d. The conductivity and derived salinity and density profiles shown in figures 7 b-d look "reasonable" with no evidence of density inversions seen earlier in figure 2 d, even though the default time constant value is slightly low (i.e. t = 0.94 versus our estimate of 1.09 s.). The April 3 EXCELL data are associated with the microstructure probe example shown earlier in Figures 2 a-d.

The lagging procedure leaves the temperature unchanged and a least squares estimate of the temperature lag, shown in figure 8a, gives a slightly better response time of t = 1.09 s (model response is squares) while observations are marked as asterisks (*).

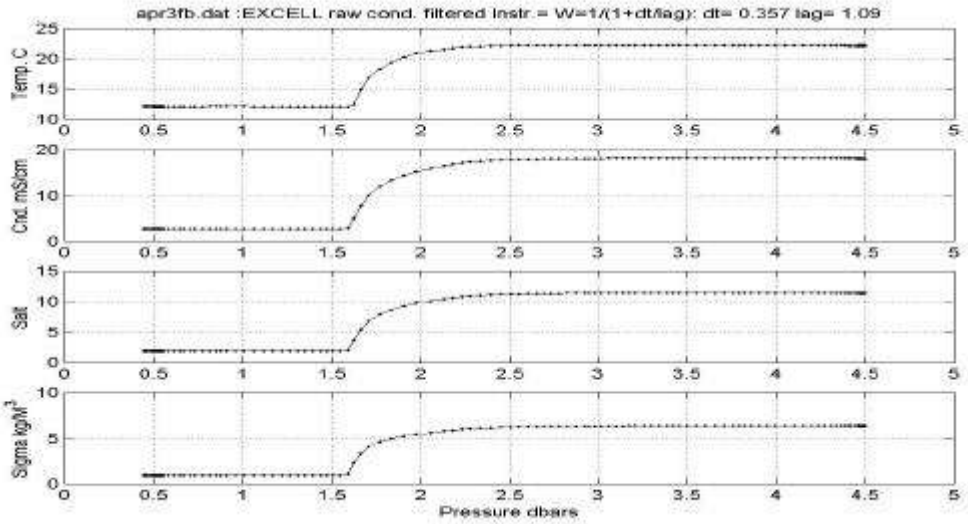

Figure 7 a-d Four panel plot of temperature, conductivity, salinity, and density versus pressure from the 2nd April 3, 2000 plunge of EXCELL # 1321. The instrument default filtering with t =0.93 s has been applied to conductivity and pressure.

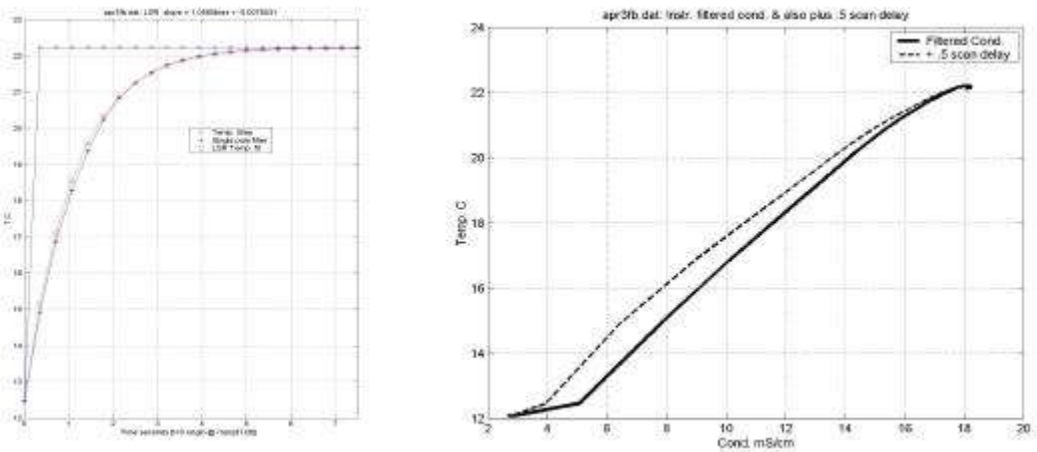

Figure 8a, gives a lag t = 1.09 s (model response is squares) while temperature observations are indicated by asterisks (*). Figure 8b "Figure of merit" plot of C versus T. (Solid) is observed instrument conductivity while (dashed) has a 0.5 scan (0.179 s) delay added to the conductivity, since its external field senses the interface prior to the thermometer.

A useful "figure of merit" for dynamic response studies involves plotting temperature versus conductivity for a given run. The form of the transition from one T, C value representing the cold fresh, upper layer to that of the warm, salty, lower layer reveals much about the character of the T and C sensor dynamic response (Figures 8.b, 9.a, 9.b). A slow thermometer is apparent as a concave curve, and various lags and filtering can be applied to achieve the ideal straight-line response of the system between the two layer properties. A straight line, such as the dashed C/T curve adjusted by a lag of 0.5 scans in figure 8.b, reveals properly matched T and C sensors and assures that averaging to coarser resolution will yield an accurate estimate of the average properties. A simple time lag due to physical positioning or sampling sequence appears as a delayed temperature response (concave upward at the start of the run at low T, C). Effects due to the thermal mass of the conductivity cell appear as a delayed conductivity response as high T, C values in the lower layer are approached.

3.7 Thermal Mass Effect

Lueck (1990) and Lueck and Picklo (1990) describe the thermal mass effect of conductivity cells. Because of the heat capacity of the cell, the temperature and thus the conductivity of the fluid in the measurement volume is altered by the presence of the cell. In our case the low temperature of the cell on passing through the interface causes a decrease in the measured conductivity, seen as a curvature in the C-T plot near the high C, T values of the lower layer (Figure 9.b), as the measured conductivity more slowly approaches the layer value. Lueck (1990) finds that the thermal mass problem can be addressed by adding in a correction to the conductivity record that is proportional to the time rate of change of temperature. This can be applied as a discrete filter:

$$\begin{aligned} C_c(i) &= C_f(i) + C_T(i), \\ C_T(i) &= bC_T(i-1) + a(T_l(i) - T_l(i-1)). \end{aligned} \qquad (3.10)$$

Here the thermal mass correction is represented by C_T, the filtered conductivity by C_f , and the corrected conductivity by C_c . The magnitude of the correction (C_T) depends on the rate of change of lagged temperature (T_l) through a coefficient (a) proportional to the temperature dependence of conductivity, the sampling rate, and the thermal anomaly generated by the cell, plus a memory term (b) proportional to the thermal mass of the cell, that determines how long the thermal correction is applied.

For the FSI EXCELL head we find little need for a thermal mass correction at the 10 –15 cm/s speed of a float, but do find lagging and thermal mass corrections useful at higher translation speeds. Figure 9.a shows diagnostic conductivity- temperature plots for slow speed (~12 cm/s) runs with and without the standard conductivity filter applied. Figure 9.b shows a higher speed run (~30 cm/s) with default conductivity filter only and with a fractional lag of the conductivity relative to temperature plus the thermal mass correction, with the weights a and b chosen by inspection. As Lueck (1990) notes, complete characterization of the conductivity and temperature responses of a conductivity cell is theoretically impossible because of the differing salinity and temperature boundary layers. However, for CTDs with finite sampling rate and noise levels, the algorithms given above provide a method for optimizing the performance of the sensor system that should prove satisfactory in most applications.

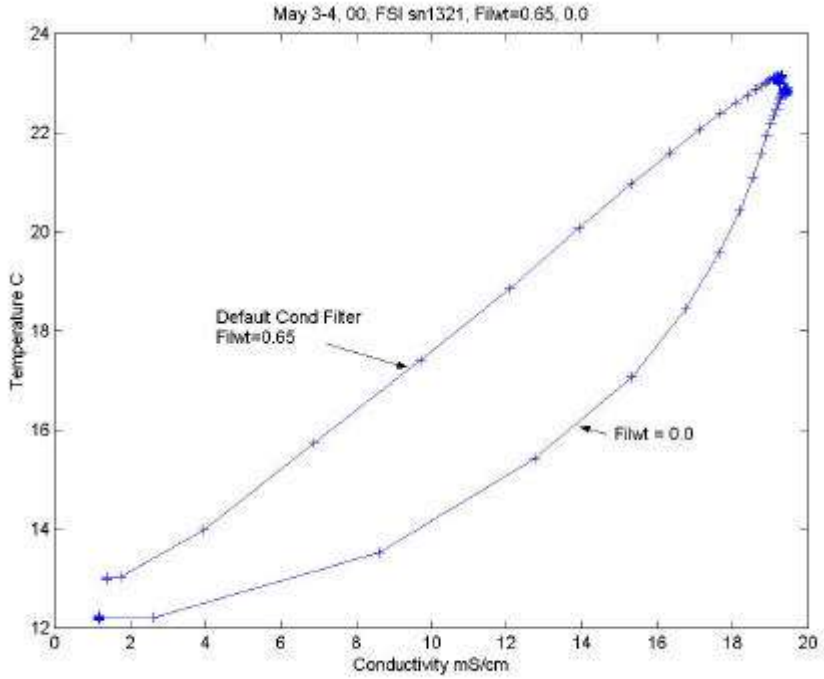

Figure 9.a The performance of FSI EXCELL 1321 on two separate days, with and without the default conductivity filter applied. These were run at speeds of ~12 cm/s, where the standard filter is seen to perform well, yielding a reasonably straight C-T line between the values of the two mixed layers. Note the temperature contrast over 10^{o} C with only slight changes in layer properties over one day.

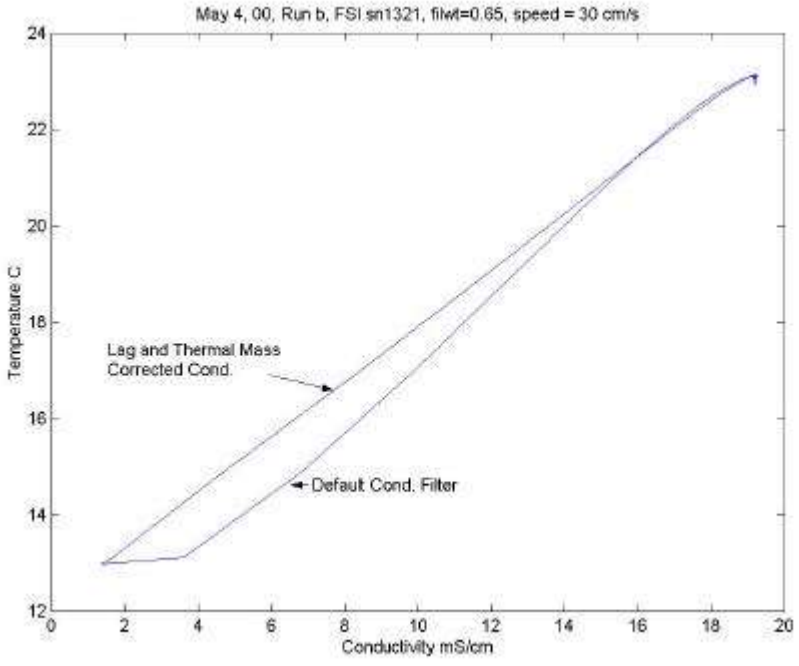

Figure 9.b A higher speed run (~30 cm/s) shows the need for lagging of the conductivity record relative to temperature, which corrects the C-T curve at the beginning of the interface (low C, T values). The thermal mass correction (with a=0.4, b=0.6) serves to straighten the C-T curve at high C, T values, where the sensor has entered the lower warm, salty layer.

4. Future Work

As presented above, the double-diffusive interface tank has been found to be particularly useful for *a priori* characterization of the dynamic response of sensors deployed on autonomous instruments where the necessity for on-board data reduction precludes *post-hoc* correction of the data. The need for speed dependent lag correction algorithms was clearly demonstrated by our limited runs at different fall rates. The conductivity–temperature plot was found to be an efficient diagnostic for identifying sensor lag, response time, and thermal mass effects. We have used the tank for performance testing of profiling floats and studies of the relative mixing rates of dissolved salts and injected tracers. Characterization of the response of optical, acoustic and microstructure sensors to double-diffusive interfaces is being undertaken. We are also implementing synchronous logging of the (slow) CTD data and the 200 Hz microstructure data. This will permit calculation of more sophisticated transfer functions for both T and C sensors, for improved estimation of the true temperature and salinity. Also, we plan to devise a mechanism to more quickly accelerate heavier test units up to the desired drop speed. Finally, we hope to test a number of popular CTDs for the dependence of sensor response on fall rate and angle of attack, so that more robust, speed-dependent lag-correction algorithms can be designed.

Acknowledgements

WHOI Summer Student Fellows Mark Szigety and David Stuebe assisted with some aspects of the tank development. This research was supported by the National Science Foundation, grant OCE-97-11869 and by a WHOI Mellon Technical Staff Award.

References

Davis, R. E., D. C. Webb, L. A. Regier, and J. Dufour, 1991. The autonomous lagrangian circulation explorer. *Journal of Atmospheric and Oceanic Technology*, **9**, 264-285.

Fofonoff, N. P., S. P. Hayes, and R. C. Millard, 1974. WHOI/Brown CTD microprofiler: methods of calibration and data handling. *Woods Hole Oceanographic Institution Technical Report*, **66**, 74-89.

Fofonoff, N. P., and R. C. Millard, Jr., 1983. Algorithms for computation of fundamental properties of seawater. *UNESCO Technical papers in Marine Science*, **44**. Unesco, Paris.

Giles, A. B., and T. J. McDougall, 1986. Two methods for the reduction of salinity spiking of CTDs. *Deep-Sea Research*, **33**, 1253-1274.

Gregg, M. C. and T. B. Meagher, 1980. The dynamic response of glass-rod thermistors. *Journal of Geophysical Research,* 85, 2779-2786.

Gregg, M. C., J. C. Schedvin, W. C. Hess, and T. B. Meagher, 1982. Dynamic response calibration of the Neil Brown conductivity cell. *Journal of Physical Oceanography*, **12** (7), 720-742.

Gregg, M. C., T. B. Meagher, E. E. Aagaard, and W. C. Hess, 1981. A salt-stratified tank for measuring the dynamic response of conductivity probes. *IEEE Journal of Oceanic Engineering*, **OE-6** (4), 113-118.

Gregg, M. C., and W. C. Hess, 1985. Dynamic response calibration of Sea-Bird temperature and conductivity probes. *Journal of Atmospheric and Oceanic Technology*, **2** (3), 304-313.

Horne, E. P. W., and J. M. Toole, 1980. Sensor response mismatches and lag correction techniques for temperature-salinity profilers. *Journal of Physical Oceanography*, **10** (7), 1122-1130.

Lueck, R., 1990. Thermal inertia of conductivity cells: theory. *Journal of Atmospheric and Oceanic Technology*, **7** (5), 741-755.

Lueck, R., and J. J Picklo, 1990. Thermal inertia of conductivity cells: observations with a Sea-Bird cell. *Journal of Atmospheric and Oceanic Technology*, **7**, 756-768.

Middleton, J. H., and T. D. Foster, 1980. Fine structure in the Halocline. *Journal of Geophysical Research*, **85**, 1118-1122.

Millard, R. C., Jr., 1982. CTD calibration and data processing techniques at WHOI using the 1978 practical salinity scale. *Marine Technology Society Conference paper.*

Muench, R. D., H. J. S. Fernando, and G. R. Stegan, 1990. Temperature and salinity staircases in the northwestern Weddell Sea. *Journal of Physical Oceanography*, **20**, 295-306.

Neal, V. T., S. Neshyba, and W. Denner, 1969. Thermal stratification in the Arctic Ocean. *Science*, **166**, 373-374.

Scarlet, R. I., 1975. A data processing method for salinity, temperature, depth profiles. *Deep-Sea Research*, **22**, 509-515.

Schmitt, R. W., 1994. Double Diffusion in Oceanography. *Annual Review of Fluid Mechanics*, **26**, 255-285.

Stern, M. E., 1960. The 'salt fountain' and thermohaline convection. *Tellus*, **12**, 172-175.

Stern, M. E. and J. S. Turner, 1969. Salt fingers and convecting layers. *Deep-Sea Research*, **16**, 497-511.

Turner, J. S., 1968. The behaviour of a stable salinity gradient heated from below. *Journal of Fluid Mechanics*, **33**, 183-200.

Topham, David R., and Ronald G. Perkin, 1988. CTD sensor characteristics and their matching for salinity calculations. *Journal of Oceanic Engineering*, **13**, 107-117.

Unesco, 1981. Background papers and supporting data on the Practical Salinity Scale 1978. *Technical Papers in. Marine Science*, **37**, Unesco, Paris.

Appendix: Filter weight estimation for slow sample rates

The recursive filter weights calculated using equation 5.2 from Bendat and Piersol (1971) do not correctly model the behavior of a single pole filter as the sampling period approaches the sensor response time. We derive here an expression for the recursive filter weights that more closely approximates a single pole filter for temperature $T(t)$ under these slow-sample-rate conditions.

To obtain the amplitude and phase response of the temperature probe with frequency (ω) we take the Fourier transform of equation (3.2) where $\hat{T}(\omega)$ denotes the Fourier transform of $T(t)$:

$$i\omega\hat{T}(\omega) = \frac{1}{\tau}\left(\hat{T}_0(\omega) - \hat{T}(\omega)\right). \tag{A1}$$

Rearranging terms yields the complex transfer function relating $\hat{T}$ to the true $\hat{T}_0$:

$$\hat{T}(\omega) = \frac{\hat{T}_0(\omega)}{(1 - i\omega\tau)} = \frac{(1 + i\omega\tau)}{(1 + \omega^2\tau^2)} \cdot \hat{T}_0(\omega). \tag{A2}$$

The phase is given by:

$$\tan\phi = \omega\tau, \tag{A3}$$

while the square of the amplitude response is given by

$$\hat{T}(\omega) \cdot \hat{T}^*(\omega) = \frac{1}{1 + \omega^2\tau^2} \cdot \hat{T}_0 \hat{T}_0^*. \tag{A4}$$

To obtain the amplitude and phase response of the recursively filtered conductivity with frequency we take the Fourier transform of equation (5.1):

$$\hat{C}(\omega) = \alpha \cdot \hat{C}(\omega) \cdot e^{-i\omega\Delta} + (1-\alpha) \cdot \hat{C}_o(\omega), \tag{A5}$$

or

$$\hat{C}(\omega) = \frac{(1-\alpha) \cdot \hat{C}_o(\omega)}{(1-\alpha \cos(\omega\Delta)) + i\alpha \sin\omega\Delta}. \tag{A6}$$

We multiply by the complex conjugate to obtain the square of the amplitude response:

$$\hat{C}(\omega) \cdot \hat{C}^*(\omega) = \frac{(1-\alpha)^2}{1-2\alpha \cos(\omega\Delta) + \alpha^2} \cdot \hat{C}_0 \cdot \hat{C}_0^*. \tag{A7}$$

The phase is given by

$$\tan\phi = \frac{\alpha \sin(\omega\Delta)}{1-\alpha \cos(\omega\Delta)}. \tag{A8}$$

For a small $\omega\Delta << 1$ (*i.e.*, low frequencies compared to the sampling rate)

$$\tan\phi \cong \frac{\alpha\omega\Delta}{1-\alpha}. \tag{A9}$$

Assuming for the moment that the conductivity measurement is ideal (*i.e.*, no phase shift or change in amplitude versus frequency, a reasonable approximation for $\omega\Delta << 1$), we can derive an expression for the weight α that matches the phase at low frequency for the conductivity recursive filter and the response of the temperature sensor by equating equations 3 and 9:

$$\omega\tau = \frac{\alpha\omega\Delta}{1-\alpha} \tag{A10}$$

Solving for α in terms of the response time, τ, and sampling interval, Δ, we obtain:

$$\alpha = \frac{1}{(1+\Delta/\tau)}. \tag{A11}$$

This formula for α compares with the expression

$$\alpha = e^{-\Delta/\tau} \tag{A12}$$

found in Bendat and Piersol (1971) and Millard (1982), which is valid for a sample interval that is short compared with the sensor lag τ (*i.e.*, $\Delta << \tau$).

Plots of the amplitude squared and phase for the single pole temperature probe model and the recursive conductivity filter using an α weight calculated by equation A12 (exponential weight) and equation A11 are shown in Figure A1. The lower panels (A1 c & d) are for the case of a sample interval (Δ=0.04 s) that is short compared to the sensor response time (τ =0.5 s, $\Delta << \tau$). For this situation, the two models exhibit amplitude and phase behavior similar to the ideal single pole filter. The upper panels (A1 a & b) are for a situation where the sample interval (Δ=1.0 s) is comparable to the sensor lag (τ =0.5 s, *i.e.*, $\Delta \cong \tau$). The exponential estimate for α overestimates the amplitude and more importantly underestimates the phase with increasing frequency, while α estimated from equation A11 tracks the phase of the single pole filter more closely although underestimating the amplitude. Since the EXCELL CTD has a sample time comparable to the temperature probe response time, we recommend that the filter weight α be calculated from equation A11 for this instrument.

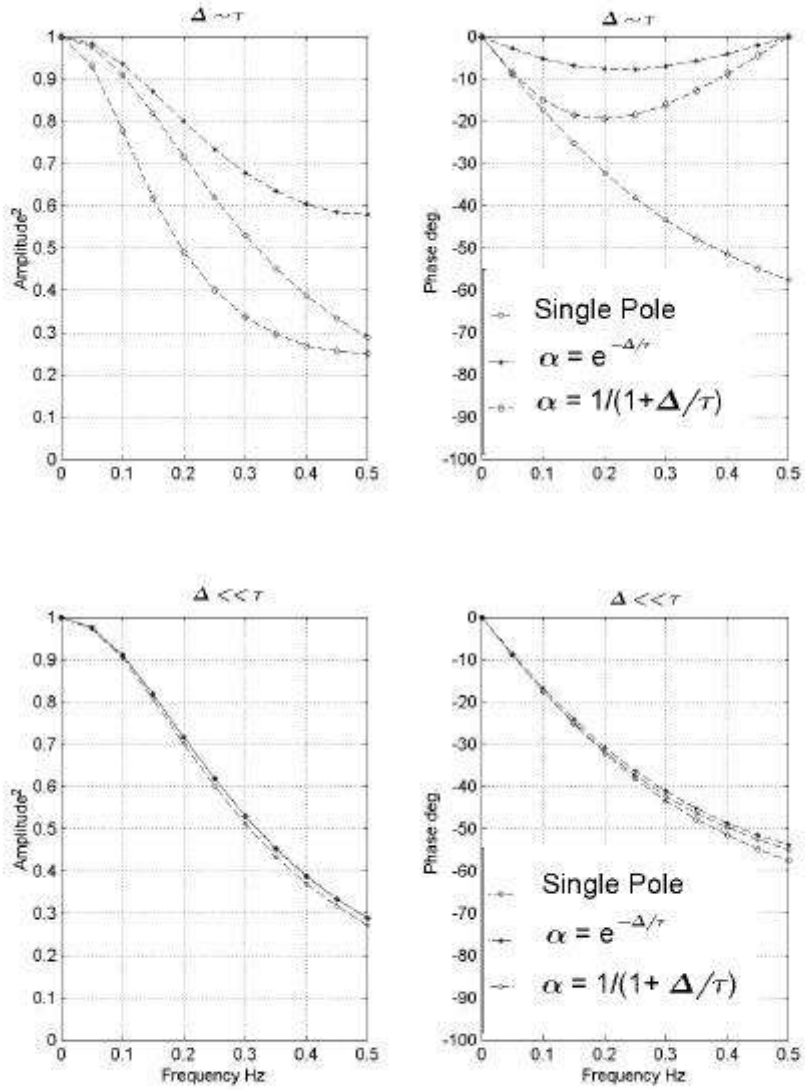

Figure A1 a & b: (upper 2 panels) Evaluation of equation 12 for the amplitude squared and equation 14 for the phase. This represents the case where the sample interval (Δ) and lag (τ) are approximately equal. Figure 10c & d (lower 2 panels) Evaluation of equation 4 for the square of amplitude response and equation 3 for the phase. This represents the case where the instrument sample interval (Δ) is much smaller than the lag (τ).